J. Phys. Chem. A **2007,** *111,* 10517−10529

Pump-Degenerate Four Wave Mixing as a Technique for Analyzing Structural and Electronic Evolution: Multidimensional Time-Resolved Dynamics near a Conical Intersection

Jürgen Hauer, Tiago Buckup, and Marcus Motzkus*

Physikalische Chemie, Philipps-Universität Marburg, Hans-Meerwein-Strasse, D-35043 Marburg, Germany

Received: May 15, 2007; In Final Form: July 11, 2007

Pump-degenerate four wave mixing (pump-DFWM) is used to simultaneously study the early events in structural and electronic population dynamics of the non-adiabatic passage between two excited electronic states. After the precursor state S_2 is populated by an initial pump beam, a DFWM sequence is set resonant with the $S_1 \rightarrow S_n$ transition on the successor state S_1. The information obtained by pump-DFWM is two-fold: by scanning the delay between the initial pump and the DFWM sequence, the evolution of the individual excited-state modes is observed with a temporal resolution of 20 fs and a spectral resolution of 10 cm^{-1}. Additionally, pump-DFWM yields information on electronic population dynamics, resulting in a comprehensive description of the $S_2 \rightarrow S_1$ internal conversion. As a system in which the interplay between structural and electronic evolution is of great interest, all-*trans*-β-carotene in solution was chosen. The pump-DFWM signal is analyzed for different detection wavelengths, yielding results on the ultrafast dynamics between $1B_u^+$ (S_2) and $2A_g^-$ (S_1). The process of vibrational cooling on S_1 is discussed in detail. Furthermore, a low-lying vibrationally hot state is excited and characterized in its spectroscopic properties. The combination of highly resolved vibrational dynamics and simultaneously detected ultrafast electronic state spectroscopy gives a complete picture of the dynamics near a conical intersection. Because pump-DFWM is a pure time domain technique, it offers the prospect of coherent control of excited-state dynamics on an ultrafast time scale.

Introduction

Time resolving structural dynamics on short-lived molecular excited states presents a challenging yet wide ranging field of ultrafast spectroscopy. The relevance of the problem is clear because such molecular modes may represent movement along the reaction coordinate and hence determine the photochemistry of the molecule. Transient absorption is a widespread technique that has proven to yield information on excited-state dynamics on a number of small systems[1,2] and molecules in solution.[3−6] A drawback of this approach is the non-trivial assignment of the observed vibrations to either ground or excited state. This can be clarified by prior theoretical knowledge of the system, which poses a limitation to small molecules. An experimental method to facilitate the assignment of vibrational modes in complex molecules is given by scanning the second-order chirp of the excitation pulse.[7,8] If the vibrational amplitude is enhanced by a negative chirp, it can be regarded as a ground-state mode.

Another aspect to be considered is the $N|\mu|^2$ dependency of the transient absorption signal[9] with μ as the rovibronic transitions dipole moment and N as the number density of the examined species. Nonlinear methods like degenerate four wave mixing (DFWM)[10−13] scale with $N^2|\mu|^8$, consequently exhibiting a radically different intensity pattern in comparison to conventional spectroscopic probes. For low concentrations of target species and weak spectral transitions, this scaling reduces the overall sensitivity of the method. For the present study of sufficiently concentrated β-carotene in solution, however, this dependence turns into an advantage given the strong transition dipole moment on both ground and excited states of this naturally occurring dye. Because of their inherent advantages, FWM techniques have been applied to a wide range of time-dependent studies of molecular vibrations since the advent of ultrashort pulses.[6,10,14−19] When applying a DFWM sequence resonant to an electronic transition from the ground state, excited-state vibrations can be observed. However, the same ambiguities concerning the origin of the vibrational modes as for transient absorption measurements apply. This can be resolved by adding an additional pump pulse prior to the DFWM sequence. Excited-state resonances can be exploited, when an appropriately set DFWM sequence only gives rise to a resonantly enhanced signal if it was preceded by an initial pump pulse. This pump-DFWM scheme[10,18] depicted in Figure 1 is a pure time domain method with a temporal resolution determined by the cross correlation between the ultrashort initial pump and DFWM pulses. The spectral resolution is only limited by the natural line widths of the vibrational features under investigation with no theoretical lower wavenumber limit. The upper limit is determined by the spectral width of the DFWM pulses.

Oberlé et al. used a similar approach to detect the excited-state population dynamics in *trans*-stilbene[20] and diphenylpolyene derivatives[21] with subpicosecond time resolution. On a femtosecond time scale, Siebert et al.[17,22] focused on hot ground-state dynamics as examined by pump-coherent anti-Stokes Raman scattering (pump-CARS). The vibrational repopulation of the ground state in all-*trans*-β-carotene was monitored. Underwood and Blank[14] introduced resonant pump, third-order Raman spectroscopy (RaPTORS), where a high intensity non-resonant DFWM sequence was employed for probing solvent dynamics. Also, in the time domain, Fujiyoshi

---

* Corresponding author. Phone: +49 6421 28-22540. Fax: +49 6421 28 22542. E-mail: motzkus@staff.uni-marburg.de.

10.1021/jp073727j CCC: $37.00 © 2007 American Chemical Society
Published on Web 10/03/2007

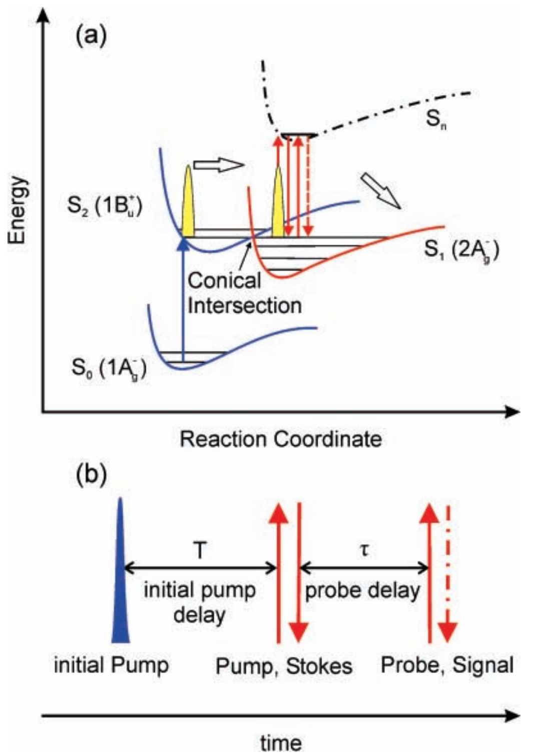

Figure 1. The pump-DFWM excitation scheme for all-*trans*-β-carotene is depicted in (a). The resonant initial pump promotes the system to the S_2 state. After an ultrafast internal conversion through a seam of conical intersections, the system relaxes toward S_1. The DFWM sequence is set resonant with the $S_1 \rightarrow S_n$ transition. Part (b) shows the time ordering of the incident pulses.

et al.[19] observed the low-frequency vibrations of *trans*-stilbene on its first excited state, employing a time-resolved impulsive stimulated Raman scattering (TR-ISRS) setup.

Another set of methods for detecting excited-state modes exploits vibrationally induced absorbance changes (Raman gains) in a broadband probe signal.[23−25] In principle, a photogenerated species is vibrationally excited by either a spectrally broad[24] or a narrow band Raman pump pulse.[23,25] The vibrational modes are detected as absorption gains on a probe pulse at the respective frequency shifts. Such time-resolved Raman scattering techniques exhibit fast data acquisition rates in combination with high spectral and temporal resolution, below 50 fs according to the review by Kukura et al.[25] Pump-DFWM, however, offers an additional spectral axis to the signal: because the vibrations are recorded in the time domain, vibrational spectra can be obtained at different detection wavelengths. Hence, spectrally dispersing the DFWM signal offers valuable new insight. Structural information recorded at different spectral cuts through the signal (see the subsection on data collection) can be compared. Frequency domain and related techniques cannot offer this perspective because the detection wavelength is not a degree of freedom. This advantage makes pump-DFWM a method presenting the unique combination of multidimensional information on structural (vibrational) and electronic population dynamics. This linkage is of special interest at points of electronic degeneracy like conical intersections.[26,27] To demonstrate the ability of pump-DFWM to dissect the dynamic behavior near such a decisive point of a potential energy surface, the conical intersection between the first two excited states in all-*trans*-β-carotene in cyclohexane was chosen. The ultrafast dynamics of carotenoids are an active field of research. For a recent summary, see the review by Polivka and Sundström and references therein.[28]

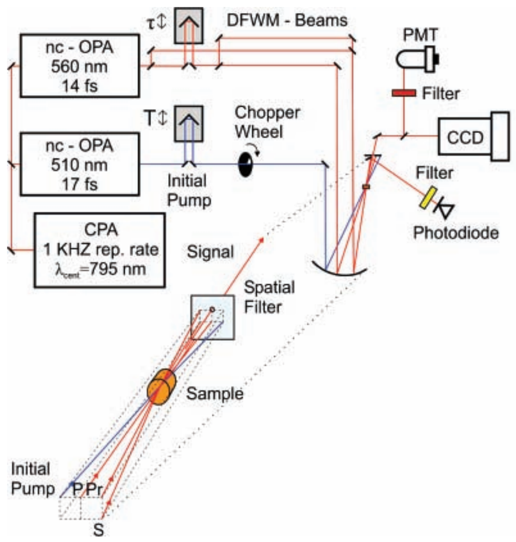

Figure 2. Experimental setup for pump-DFWM. The regenerative amplifier (CPA) pumps two nc-OPAs. The initial pump triggers the photochemistry and precedes the DFWM sequence by *T*. It is blocked periodically by the chopper wheel. The initial pump interacts with the DFWM beams at the sample in a folded BOXCAR arrangement. The probe beam (Pr) is delayed by τ to give transients recorded either in a CCD camera or in a photomultiplier tube (PMT). Transient absorption data are collected simultaneously in a photodiode (TA).

Materials and Methods

Instrumentation. The experimental setup is depicted in Figure 2. Its functionality was demonstrated as a proof of principle in a previous publication by our group.[18] In the present work, we improved the experimental parameters like spectral resolution and signal-to-noise ratio. Furthermore, the present setup allows for detection of electronic population dynamics as mentioned above.

The regeneratively amplified Ti:Sapphire laser delivered 120 fs, 700 μJ pulses at 1 kHz repetition rate, centered at 795 nm. This fundamental beam was split into two parts of equal intensity to pump two separate single staged non-collinear parametric amplifiers (nc-OPA). The initial pump (see Figure 2) was centered around 510 nm with a temporal pulse width of 17 fs as determined by an autocorrelator. The initial pump precedes the DFWM sequence by *T* (see Figure 1). The delay was set with the aid of a computer-controlled Piezo stage. Before reaching the sample, the beam went through a synchronized chopper wheel, blocking every second pulse. This allowed for discriminating between transients with (“initial pump on”) and without (“initial pump off”) the initial pump beam in Figure 2 preceding the DFWM sequence. The latter was obtained by splitting the output of another nc-OPA into three parts of equal intensity. The spectrum of the DFWM sequence (see Figure 3b) was centered around 560 nm with a duration of 14 fs fwhm. One of the three DFWM beams serving as the probe beam in the DFWM process was delayed by τ. To guarantee photostability of the solution during the course of the experiment, the intensities of all incident beams were kept as low as possible at the sample, that is, 40 nJ for the initial pump, 15 nJ for DFWM-pump and Stokes, and 3 nJ for the probe beam. All beams were horizontally polarized. Before interacting with the sample, the beams were focused by a concave mirror with 30 cm focal length, resulting in a beam radius of 40 μm in the focus. The spatial geometry of the incident beams, the so-called folded BOXCAR geometry, was chosen so that the resulting signal was unperturbed by scattering light from the other beams.[10] The signal was spatially filtered by a series of irises before it reached

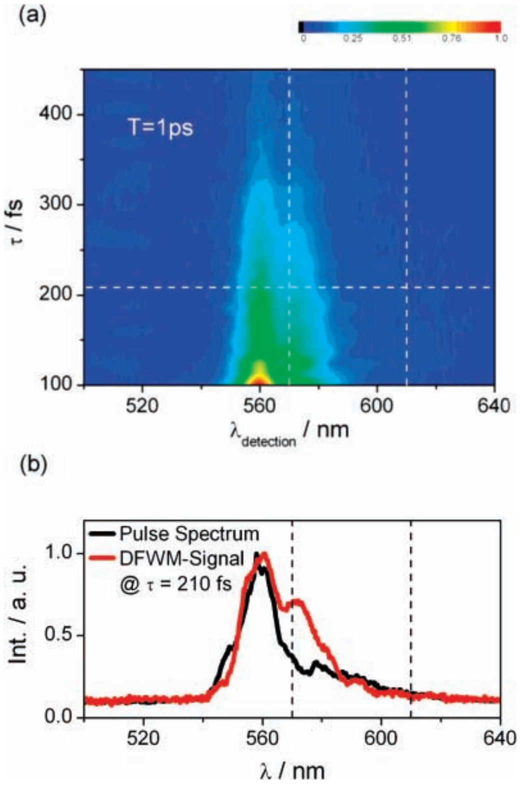

Figure 3. A typical spectrum of the pump-DFWM signal after subtraction of the signal with the initial pump blocked is shown in (a). The initial pump delay T was set to 1 ps. The vertical dashed lines mark two different detection wavelengths as discussed in the text. Part (b) shows a spectrum of one of the DFWM pulses (black line) in comparison to a DFWM signal (red line) taken at probe delay indicated by the horizontal line in (a).

the detection part of the experiment to ensure a low noise level. In the employed setup, three different detection methods were used. The DFWM signal was either detected in a photomultiplier after an interferometric filter or spectrally dispersed and recorded in a CCD camera with 1024 pixels. Even though detection by a CCD camera offers a greater wealth of information because all of the wavelengths in the signal can be recorded simultaneously, the photomultiplier proved to be the more feasible tool for long transients due to its faster data acquisition times. In the third method of detection, not the DFWM signal but the probe beam was recorded in a photodiode after the sample at a chosen wavelength. Because the initial pump was blocked periodically, this setup also allowed for a transient absorption measurement (see Figure 4b). Recording this response is important to exclude possible saturation or exceedingly big depletion effects by the DFWM sequence.

Sample Preparation. All-*trans*-β-carotene was used as received from Aldrich and dissolved in HPLC-grade cyclohexane. The optical density of the sample was adjusted to OD 1 at β-carotene's first maximum of absorption near 485 nm. The solution was placed in a 250 μm thick cell with 0.5 mm thick fused silica windows. To reduce stray light from the window's surface, the sample was kept static during all measurements. The solution showed no sign of degradation over the course of the experiment.

Data Collection. Figure 3a shows a typical CCD signal at an initial pump delay T of 1 ps. The signal with the initial pump blocked, that is, the non-resonant signal from β-carotene's ground state, is already subtracted. The strong coherence peak[29] around $\tau = 0$ fs is omitted for clarity.

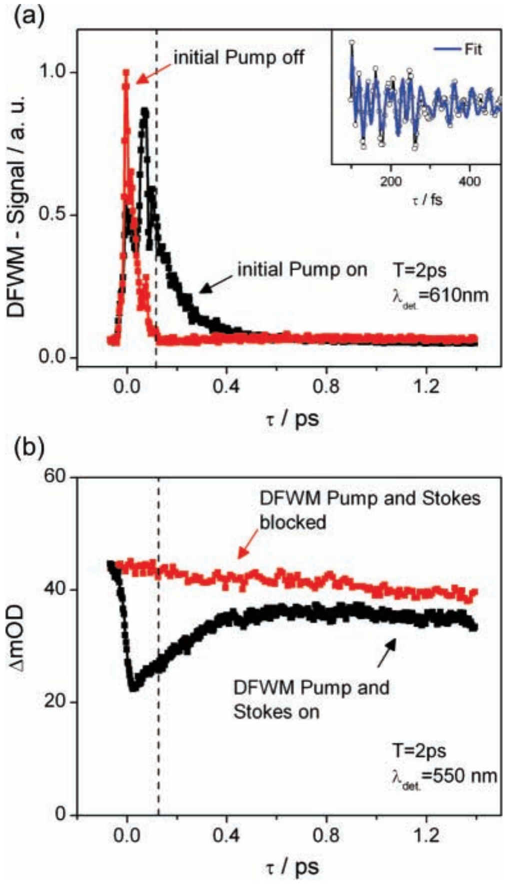

Figure 4. Transients with (black line) and without (red line) the initial pump beam preceding the DFWM sequence are shown in (a). The exponential decay of the signal in the former case indicates a resonant process. The data were taken at an initial pump delay $T = 2$ ps. The dashed line marks the time window around the coherence peak, which was not taken into account in further analysis. The inset shows a fit of a sum of damped sine functions to the data after subtraction of the slow kinetics. See Table 1 for the obtained parameters. In (b), the effects of the DFWM pump and the Stokes pulse in the DFWM sequence are demonstrated on the basis of a transient absorption measurement. The sequence was kept low in intensity (15 nJ for DFWM pump and Stokes, 3 nJ for the probe pulse). This kept the population loss (final level of the data with and without the DFWM pump and the Stokes pulse) below 10%.

As expected for a $T = 1$ ps, the signal is positive throughout the window of detection, meaning that the DFWM signal is much stronger when the initial pump is on. This is due to the fact that the DFWM sequence can interact resonantly with the $S_1 \rightarrow S_n$ transition (see Figure 1) but is non-resonant with respect to the first dipole allowed transition from β-carotene's ground state ($S_0 \rightarrow S_2$). As demonstrated in theory and experiment,[30−32] resonant DFWM signals can be up to 10^6 times stronger than non-resonant ones. In Figure 3b, the signal at a probe delay of 210 fs (horizontal dashed line in Figure 3a) is compared to the spectrum of the DFWM beams. The intensity distribution is not equal between the two spectra due to the properties of the S_1 state, showing an absorption centered around 560 nm.[28] The vertical dashed lines in both plots indicate the detection wavelengths for the transients discussed in Figure 4.

By delaying the probe pulse by τ at a given initial pump delay T, transients like those in Figure 4a were obtained.[18] The role of the initial pump becomes obvious when transients with and without the pulse are compared. The data set in Figure 4a with the initial pump off shows a measurement where the initial pump was blocked by a chopper wheel (see Figure 2). The signal is dominated by an instantaneous rise around $\tau = 0$ fs

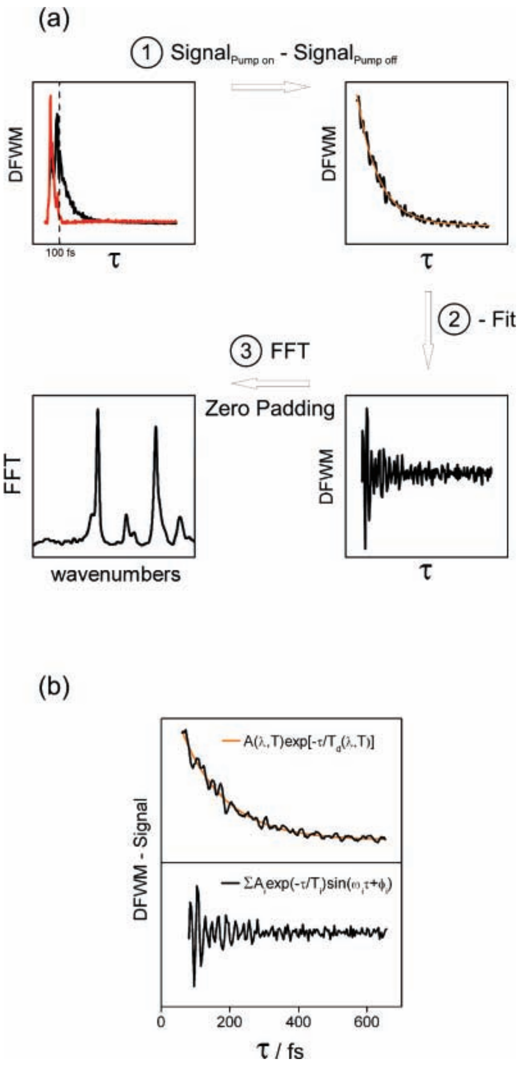

Figure 5. Summary of the data analysis procedures in (a). After subtracting the signal with the initial pump on from the signal with the initial pump off and exclusion of the coherence peak (step 1), a slow exponential decay is fitted to and subtracted from the data (step 2). Fast Fourier transformation (FFT) after zero padding leads directly to a vibrational spectrum (step 3). In (b), the variables used for describing the non-oscillatory (upper panel) and oscillatory part (lower panel) are summarized.

followed by a rapid decay. Superimposed on this decay, there are fast oscillations with lifetimes and amplitudes summarized in Table 1. The spectra of the pulses in the DFWM sequence (see Figure 3b) show no overlap with the $S_0 \rightarrow S_2$ absorption band. This leads to the conclusion that in the absence of the initial pump, only ground-state (S_0) oscillations are addressed via a non-resonant excitation mechanism.[18,32] Accordingly, the fast decay of the red line in Figure 4a with the initial pump blocked can be attributed to the rapid dephasing of a non-resonant DFWM signal. The situation is fundamentally different if the initial pump is allowed to interact with the sample prior to the DFWM sequence (see black line in Figure 4a). After a coherence peak around $\tau = 0$ fs, the signal decays much more slowly (114 fs) as compared to the case where the initial pump is off (40 fs). This is explained by lifetime-related terms in the overall decay time T_d for resonant DFWM signals, missing for non-resonant interactions.[9,33] The blue line in the inset represents a fit to the data after subtraction of the slow kinetics and the data with the initial pump blocked. The details of this analysis procedure will be dealt with in Figure 5a. At the present stage of the discussion, it is important to note that the molecular vibrations appear as oscillations of the DFWM signal, superimposed on a slowly decaying background.

Multiphoton excitation leading to higher lying excited states from the ground state during non-resonant interaction with the DFWM sequence can be neglected due to the low excitation energies used (15 nJ for the DFWM sequence's pump and Stokes and 3 nJ for the probe pulse). To further sustain the exclusion of multiphoton processes, the effects of the DFWM pump and the Stokes pulse were monitored simultaneously by a transient absorption measurement. Figure 4b compares two such transients, one with (black line) and one without the DFWM pump and the Stokes pulse. Because the initial pump precedes the other pulses by $T = 2$ ps, no coherent artifact around $\tau = 0$ fs is expected for the probe-only data set. The signal is dominated by a 9 ps decay, which is typical for β-carotene's S_1 state.[28] When the DFWM pump and the Stokes pulse are allowed to interact with the sample at $\tau = 0$ fs, however, the $S_1 \rightarrow S_n$ transition centered around 560 nm causes the signal to decrease instantaneously. This process is followed by a rapid increase with a 310 fs rise time, which is attributed to an internal conversion from S_n back to S_1. This process is not loss free, which explains the difference between the signal with and without the DFWM pump and Stokes pulse at later probe delay times. In pump−repump−probe experiments[34−36] on β-carotene, a similar net loss of population was reported. This effect was accounted for by the formation of a radical. This species does not absorb in the spectral window observed in the current experiment, leading to an apparent loss in population. Importantly, the decay time after the repopulation process (9 ps) is equivalent to the probe-only decay. This strongly suggests that the population returns to the S_1 state. The linearity of the transient absorption signal with respect to the initial pump's energy (40 nJ) was also ensured.

To examine β-carotene's excited-state structural evolution while excluding non-resonant contributions from the ground state, a straightforward procedure is applied (see Figure 5 for a summary). With the purpose of acquiring transients unperturbed by the coherent artifact around $\tau = 0$ fs, only data points for $\tau \geq 100$ fs were considered (see dashed line in Figure 4a). Next, the non-resonant transient was subtracted to reveal information on the excited state only. Because the non-resonant signal is expected to oscillate $\pi/2$ out of phase with the resonant contribution after interaction with the initial pump pulse, no constructive or destructive interference between the two components will occur.[37] Hence, a simple subtraction suffices to

TABLE 1: Fitting Parameters According to an Evolutionary Fitting Routine Based on $\mathrm{Signal}_{\mathrm{DFWM}}(t) = \sum_i A_i e^{t/T_i} \sin(\omega_i t + \phi_i)$

	$\lambda_{\text{detection}} = 610$ nm				$\lambda_{\text{detection}} = 570$ nm			
	A_i	ω_i/cm^{-1}	T_i/fs	ϕ_i/rad	A_i	ω_i/cm^{-1}	T_i/fs	ϕ_i/rad
C═C stretch S_1	1 ± 0.3	1814 ± 5	150 ± 50	0 ± 0.1				
C═C stretch	1 ± 0.1	1524 ± 2	260 ± 20	0 ± 0.07				
C−C stretch	0.6 ± 0.1	1150 ± 5	270 ± 40	−0.7 ± 0.3	0.1 ± 0.02	1160 ± 3	260 ± 30	1.4 ± 0.4
cyclohexane (solvent)	0.7 ± 0.1	800 ± 1	440 ± 40	−1.44 ± 0.06	0.1 ± 0.01	802 ± 0	280 ± 10	3.03 ± 0.07
torsional mode					1 ± 0.1	100 ± 23	250 ± 40	1.9 ± 0.2
low-frequency mode					0.9 ± 0.2	42 ± 1	80 ± 20	4 ± 2

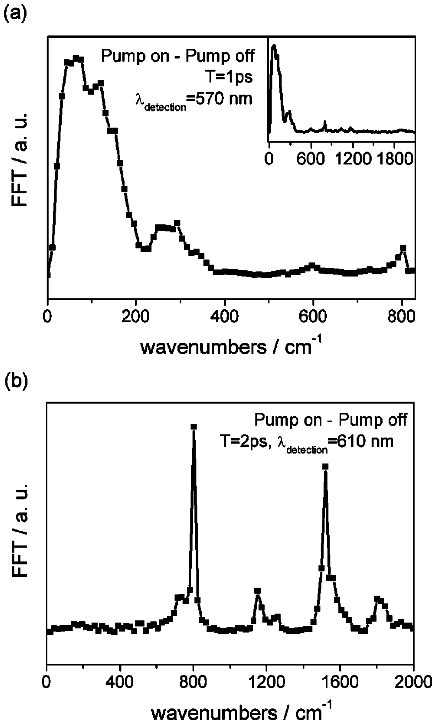

Figure 6. Comparison between two FFT spectra taken at different detection wavelengths. When detected close to the DFWM signal's maximum like in (a), the dominant spectral features are to be found in the low wavenumber region. Further detuned from the signal's maximum (compare to vertical dashed lines in Figure 3), vibrational features at much higher frequencies become apparent as seen in (b).

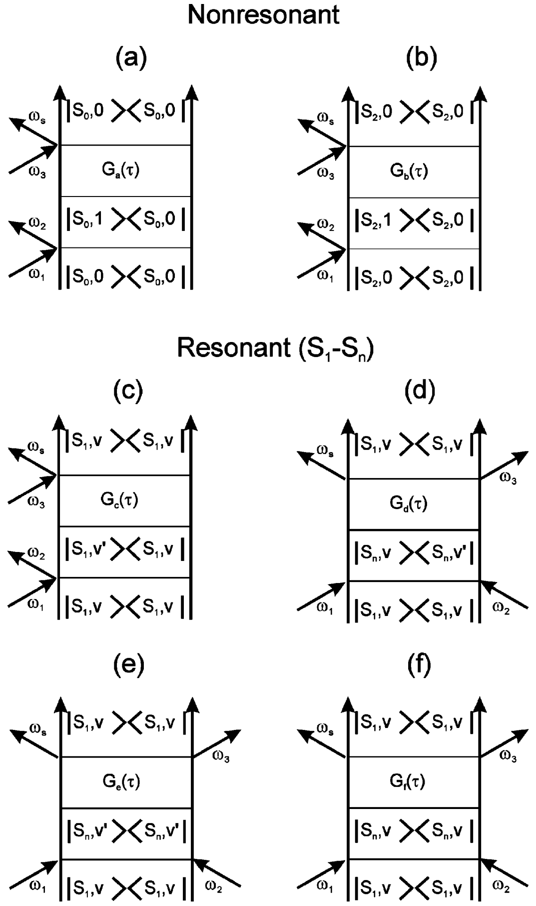

Figure 7. Feynman diagrams for the DFWM signal at the direction $k_s = k_1 - k_2 + k_3$. $G_x(\tau)$ represents the evolution of the system after the excitation with the DFWM pump and the Stokes pulses. Depending on the diagram, $G_x(\tau)$ represents different evolutions: (a) vibrational coherence in the ground state S_0, (b) vibrational coherence in the second excited state S_2, (c) vibrational coherence in the first excited state S_1, (d) vibrational coherence in the S_n state, (e) vibrational, and (f) electronic population in the S_n state.

remove the non-resonantly excited ground-state modes. The oscillatory features are up to a factor of 500 stronger when the initial pump is on, depending on the initial pump delay T. To subtract the signal's slowly varying background, a single-exponential decay was fitted to the data as indicated by the orange line in Figure 5a after step 1. A single decay rate sufficed to describe the non-oscillatory part of the signal. This is in agreement with the model given by Joo and Albrecht,[33] which will be discussed in the theoretical basis section. As a final step, fast Fourier transformation (FFT) after zero padding leads to vibrational spectra like those in Figure 6. Zero padding increases the length of the data set to be Fourier-analyzed to the next bigger power of two by adding a sequence of zero-valued data points. This procedure is needed to efficiently perform an FFT but does not alter the spectral resolution of the signal, which is determined by the length of the transient against the probe delay τ. Whenever spectral resolution is discussed in this Article, it is referred to the data set before zero padding as determined directly in the experiment. Figure 5b gives a summary of the symbols used in the discussion. The slowly decaying, non-oscillatory part of the signal depicted in the upper panel of Figure 5b is best described by a monoexponential decay with $A(\lambda,T)\ \exp[-\tau/T_d(\lambda,T)]$. The wavelength and time dependences of the pre-exponential amplitude $A(\lambda,T)$ and the overall decay constant $T_d(\lambda,T)$ will be discussed below. The oscillating part in the lower panel of Figure 5b is reproduced satisfactorily (see inset in Figure 4a) by a sum of damped sine functions. The results of this fitting procedure will be discussed in the Results and Discussion.

Because pump-DFWM is a pure time-domain method, the spectral resolution can be optimized until it is only limited by the intrinsic physics of the sample, rather than by instrumental boundaries.[38] In Figure 6a, a spectral resolution as low as 10 cm^{-1} is realized, as determined by the length of the employed Piezo stage. Hence, the factor determining the shape of the FFT spectra is not the achievable spectral resolution but the natural line width of the excited state's spectral features. Figure 6b shows a transient taken at 610 nm detection wavelength with a resolution of 20 cm^{-1}. The signal-to-noise ratio in this case is 6.0. When detected at 570 nm (Figure 6a) this ratio becomes 4.5. This difference is explained by the position of the respective detection wavelengths relative to DFWM signal's central wavelength (see Figure 3a): because detection at 570 nm is close to the maximum at 560 nm, stray light reduces the signal-to-noise ratio. When the vibrational spectra are recorded at different initial pump delays T (see Figure 9), the temporal resolution is only limited by the cross correlation of the initial pump and the pulses of the DFWM sequence. The achieved temporal resolution was 20 fs, as determined by a measurement in a 0.5 mm fused silica window.

Theoretical Basis. To describe the possible contributions to the signal in the direction $k_s = k_1 - k_2 + k_3$ (BOXCAR geometry), the corresponding Feynman diagrams are shown in Figure 7. The possible non-resonant contribution to the signal stems from the ground-state S_0 (Figure 7a) and, after the excitation with the initial pump, from the excited state S_2 (Figure 7b), both dominated by vibrational coherences. The non-resonant signal from the ground state was already investigated in our group.[32] In the current setup, it is subtracted for every data point as explained in the previous section. Non-resonant contributions

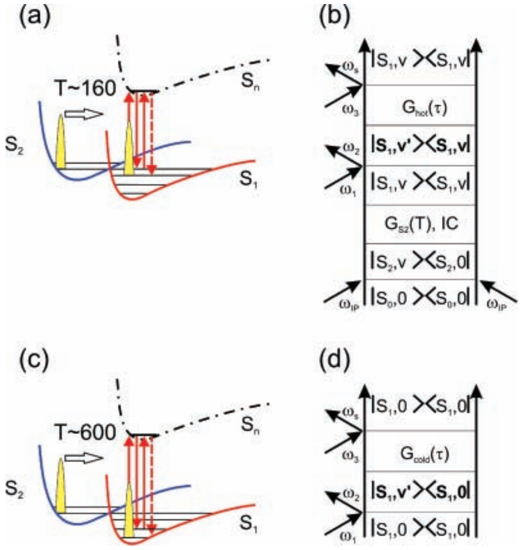

Figure 8. The effect of population flow from a vibrationally hot S_1 state to cold S_1 on the induced polarization. For early delays T between the initial pump and the DFWM pump and Stokes pulses (a and b), the non-oscillatory signal decays with a component proportional to the coherence decay time for vibrationally hot S_1 states ($T_{2,S1,\upsilon}/2$). IC stands for internal conversion. For later delays $T > 600$ fs (c and d), the signal will be determined by the loss of coherence of cooled vibrational levels on S_1 ($T_{2,\upsilon=0}/2$).

from the S_2 state are only to be expected for initial pump delay times T below 160 fs, which corresponds to the state's electronic lifetime.

The resonant signal from the S_1 state contains several contributions: Figure 7c and d represents vibrational coherences in the S_1 state and in the S_n state, respectively. Figure 7e and f depicts the contribution from vibrational and electronic population of S_n.

The usual theoretical approach to model the DFWM signal is to solve the Liouville equation perturbatively up to the third order and then calculate the third-order polarization.[13] Joo and Albrecht[33] already discussed the decay time of each of the possible contributions shown in Figure 7. The DFWM signal can be separated into oscillating and non-oscillating terms (see Figure 5a). The oscillating part originates from the coherent superposition of vibrational levels in each electronic state (S_1 and S_n) depicted in Figure 7c and d, respectively, and decays proportionally to the vibrational dephasing time $T_{2,\upsilon}$ for each state. The frequency of the observed oscillations corresponds to the vibrational modes found in the electronic states. The non-oscillating part of the signal shows contributions from different terms: (i) the real populations (Figure 7e) and (ii) the vibrational coherent superposition in the S_1 state (Figure 7c) and in the S_n state (Figure 7d). Therefore, the monoexponential decay of the DFWM signal (see Figure 4a) is composed of the electronic population lifetime from S_n ($T_{1,Sn}/2$, see Figure 7f), the vibrational population lifetime in S_n (Figure 7e) ($T_{1,Sn,\upsilon'}/2$), and the vibrational dephasing time ($T_{2,\upsilon}/2$) at each state, S_1 and S_n. For early initial pump delay times T, all four diagrams (Figure 7c−f) may contribute equally to the signal. For later delay times, however, the contributions from the population as well as from the vibrational part of the S_n related signal have decayed (see Figure 4b), leaving Figure 7c as the only influential diagram.

Because of the different time scales determining the pump-DFWM transients in β-carotene, the relaxation of S_2 toward the S_1 state and the following vibrational cooling in S_1 deserve a more detailed discussion. In β-carotene's photochemistry, the first step is excitation of S_2 from the ground state by a single photon from the initial pump pulse. Afterward, the excited molecule undergoes an ultrafast relaxation to a highly excited dark S_1 state. In solution, this process occurs within 160 fs. The cooling of vibrationally hot S_1 state takes place on a slower time scale (400 fs). Because the DFWM pulses are only resonant with the S_1 absorption, the DFWM signal has stronger or weaker contributions from excited vibrational levels on S_1 depending on the delay T between the initial pump and the DFWM sequence. This means that the DFWM signal at early initial pump delays 180 fs $\leq T \leq$ 400 fs stems from excited vibrational levels of the S_1 state. For later delay times T, the population has already relaxed to lower vibrational levels. In the former case (Figure 8a), the initial-pump populating S_2 and the subsequent internal conversion (IC, see Figure 8b) may play a role. After the non-adiabatic passage toward S_1, the decay time of the non-oscillating DFWM signal will be determined by the dephasing of coherently excited high-lying vibrational levels on S_1 ($T_{2,S1,\upsilon}/2$). For later delays in T (Figure 8c and d), the influential term is related to a coherence of vibrationally cooled states on S_1 ($T_{2,S1,\upsilon=0}/2$).

For $T = 0$ fs, the initial pump overlaps with the DFWM pump, and Stokes pulses and higher order excitations may occur. These contributions are not discussed because they are only detectable in phase matching direction different from the one employed in the experiment.

Results and Discussion

Pump-DFWM allows for multiplexed detection of vibrational modes. It gives information on vibrational and electronic dynamics as well as on the interplay between them. Accordingly, the following section is divided into a vibrational dynamics and an electronic population dynamics part. In the former, the structural evolution at a certain detection wavelength will be discussed in detail. In the latter, the non-oscillatory part of the signal will be compared for several detection wavelengths. The combination of these sets of data analyzed at the end of section 2 will provide a comprehensive picture of the non-adiabatical passage between the S_2 and the S_1 state. Special emphasis will be placed on the process of vibrational dephasing.

1. Vibrational Dynamics. In Figure 6, another intrinsic advantage of pump-DFWM over frequency domain and related Raman-gain methods becomes apparent. In the latter, vibrational features appear as net gains or losses at spectral positions characteristically shifted from the frequency of the scattered light. Pump-DFWM being a time-domain technique, however, bears an additional spectral axis. Molecular oscillations may occur at every detection wavelength for a spectrally dispersed pump-DFWM signal (see dashed vertical lines in Figure 3a). Numerical simulations and experimental works[39,40] readily reveal that the signal depends on the respective position along the spectral axis.[41] High-frequency modes are to be expected at large detunings to either the red or the blue side of the DFWM signal's central frequency. This can be understood intuitively by assuming that at low detunings frequency pairs with small energy differences are present, leading to excitation of modes lower in wavenumber. For the pulse lengths employed in the experiment, this means that by choosing an appropriate detection wavelength, vibrational modes up to almost 2000 cm^{-1} can be observed without any lower wavenumber limit. Accordingly, the spectrum obtained at 610 nm shown in Figure 6b mainly consists of high-frequency modes. All spectral features are unambiguously assigned to polyene vibrations.[42] The mode around 1800 cm^{-1} is characteristic of β-carotene's S_1 state.[43] The mode near 800 cm^{-1} stems from the solvent cyclohexane.

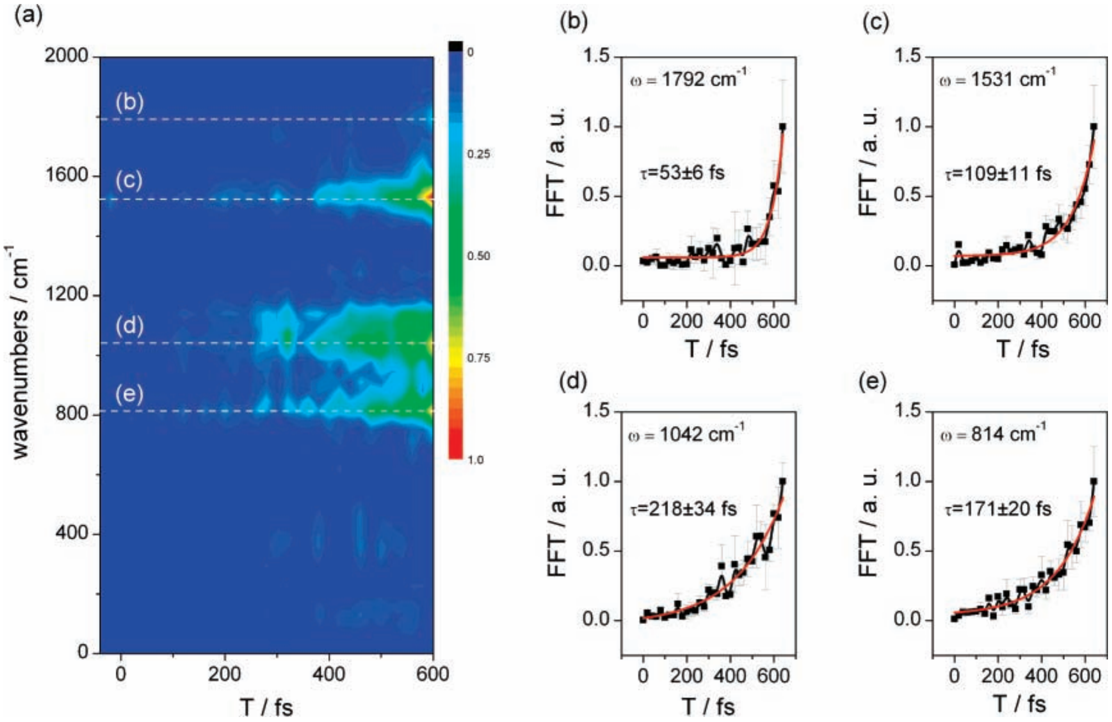

Figure 9. FFT spectra, taken at different initial pump delays T and detected at 610 nm, are shown in (a). Parts (b−e) represent cuts at indicated wavenumbers. Red lines represent monoexponential growth fittings.

Interestingly, this feature is not present when the measurement is carried out in the pure solvent. Hamaguchi et al. report a similar effect in a hyper-Raman (HR) scattering experiment on β-carotene solvated in cyclohexane.[44] Like in the experiment under discussion, a mode attributed to cyclohexane was observed, which only occurred in the presence of the solute β-carotene but was missing in the neat solvent. The authors ascribed this effect to a solvent-induced molecular near field, giving rise to an extra HR band. Even though different symmetry-based selection rules apply for a DFWM process, a similar interpretation of the Raman mode near 800 cm^{-1} can be given, because electronic resonance plays a fundamental role: as demonstrated in a DFWM study conducted in our group, the solvent mode under discussion is only observed after resonant excitation and is missing under non-resonant conditions.[32] Furthermore, the phase of the mode under discussion also deviates from resonantly excited carotenoids vibrations, as will be discussed below (see Table 1).

Shifting the detection wavelength from 610 nm closer toward the signal's maximum around 560 nm gives access to a fundamentally different range of vibrational frequencies (see Figure 6a). At 570 nm, a broad distribution of vibrations around 100 cm^{-1} dominates the spectrum, while the high-frequency modes apparent at 610 nm detection are no longer present (see inset in Figure 6a). Such low-frequency modes play a fundamental role in the energy relaxation pathway of polyenes in protein matrices.[45,46] In Table 1, a quantitative comparison of the spectra at different detection wavelengths is given. The values were fitted with an evolutionary algorithm, which was discussed in detail elsewhere.[47] A model based on $\text{Signal}_{\text{DFWM}}(t) = \sum_i A_i e^{t/T_i} \sin(\omega_i t + \phi_i)$ was used. This simple and intuitive approach treats the molecular vibrations as a sum of damped sine functions with individual amplitudes A_i, amplitude decay times T_i, frequencies ω_i, and phase terms ϕ_i. The decay time T_i can be expressed as $T_i = T_{2,\text{S1},\upsilon}$ for the respective mode, according to the formalism introduced in the theoretical basis section. The error bars represent standard deviations and are obtained by averaging 10 runs of the algorithm after reaching convergence. The obtained frequency values are within reasonable agreement with values known from literature.[48] Interestingly, for detection at 610 nm, the values for the phase terms ϕ_i are similar for all carotenoid vibrations. The mode associated with cyclohexane, however, is shifted by approximately $-\pi/2$, indicating a non-resonant excitation mechanism.[37] For detection at 570 nm, the values for ϕ_i are less meaningful, because the $S_1 \rightarrow S_n$ electronic resonance at 560 nm introduces a complex phase behavior.

The spectra in Figure 6 were obtained at fixed initial pump delays T. Scanning this parameter at a fixed detection wavelength allows for observing the temporal evolution of the molecular modes on excited energy surfaces. In Figure 9, such a scan illustrates β-carotene's structural dynamic around its conical intersection near 160 fs.[49−52]

An important feature in Figure 9a is the absence of modes with feasible intensity at early delay times below 200 fs. Considering the model for the electronic states in β-carotene given in Figure 1, this is explained by the different resonance conditions for the DFWM sequence for different initial pump delays T: if the initial pump precedes the DFWM sequence by less than 160 fs, the population is still on S_2. This initially populated state absorbs in the near infrared.[52,53] The DFWM signal originating from this energy surface is therefore not expected to experience any resonance enhancement, because the employed DFWM sequence is centered around 560 nm (see Figure 3b). On the contrary, once the system evolved through the conical intersection and populates a vibrationally hot S_1 state, the resonance condition is fulfilled, leading to a resonantly enhanced signal. The S_1 modes depicted in Figure 9b−e all exhibit individual growth times. The solvent mode shown in Figure 9e has to be viewed independently, because it is not directly affected by the $S_2 \rightarrow S_1$ seam of conical intersection. This line of degeneracy between the two states is displaced along the C═C normal mode as predicted by theory.[50,54] The modes in Figure 9c and d exhibit growth times in good agreement with

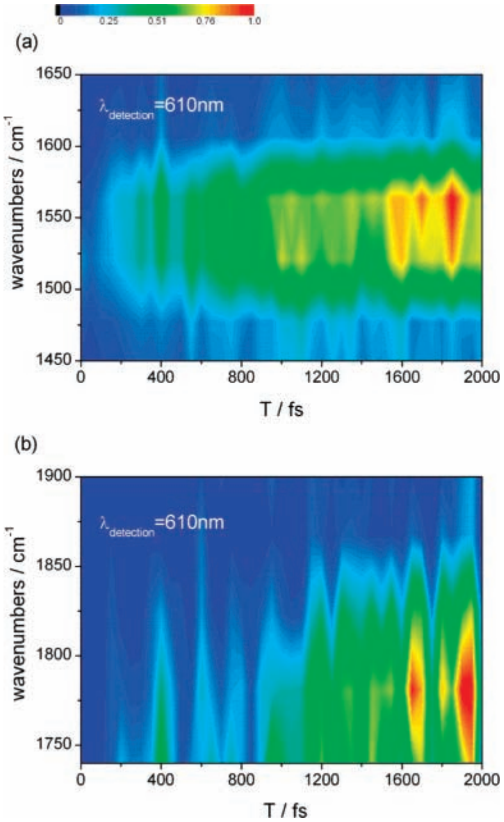

Figure 10. Structural evolution on β-carotene's S_1 state on a 2 ps time scale. Part (a) shows the gradual increase of the mode near 1540 cm^{-1}. The color code is set relative to the maximum in each plot. In comparison, the C═C mode near 1800 cm^{-1} in (b) only gains intensity at later times.

the S_2 lifetime as established in transient absorption studies.[52] The fact that a monoexponential growth fully describes the temporal behavior of the modes in Figure 9b−e illustrates that a two-level model ($S_2 \rightarrow S_1$) suffices to explain β-carotene's early excited-state dynamics, as recently argued by Kosumi et al.[53] On the basis of the data presented here, any contribution from possible intermediate states[55,56] can be disregarded.

The S_1-specific C═C mode around 1800 cm^{-1}, however (see Figure 9b), reveals a rise time much faster than those for the other modes (53 ± 6 fs as compared to values above 100 fs). The lack of a S_2-typical time constant is explained by the fact that this mode is exclusively found on S_1.[51] The delayed but then rapid gain in intensity for the S_1 C═C mode is attributed to anharmonic coupling. This means that the orthogonality between the highly excited modes breaks down, leading to a gain in energy for the initially unpopulated mode near 1800 cm^{-1}. It therefore gains intensity only after the other nuclear degrees of freedom were populated in high quantum numbers on S_1. On a longer time scale (see Figure 10b), the mode near 1800 cm^{-1} is only to be observed at later initial pump delay times T as compared to the gradual increase in intensity for the C═C stretch mode near 1530 cm^{-1} in Figure 10a. McCamant et al. proposed a similar mechanism but observe two IVR time constants, 200 and 450 fs.[43] The discrepancies from the present study are ascribed to (i) the shorter time window examined in this work and (ii) to the different excitation conditions. McCamant et al. used a picosecond Raman pump centered at 793 nm, resonant with $S_2 \rightarrow S_m$ but off resonant to the $S_1 \rightarrow S_n$ transition, where the DFWM sequence employed in the present study is on resonance. This fundamental difference leads to an alternation in the active Franck−Condon region, which serves as a possible explanation for the deviant IVR behavior.

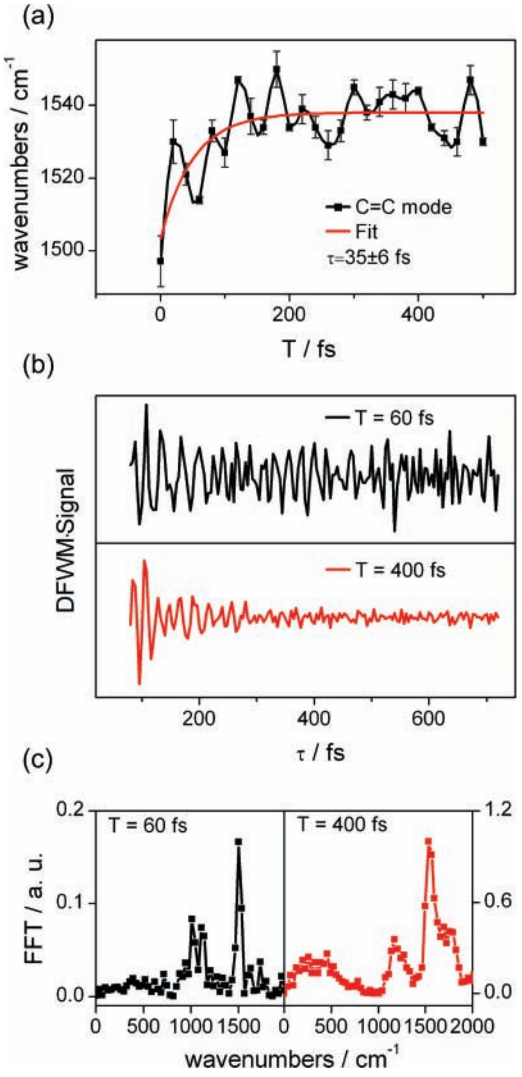

Figure 11. Part (a) shows a blue shift of the C═C stretch mode after internal conversion from S_2. Part (b) depicts the comparison between the DFWM signal's oscillatory part at $T = 60$ fs and $T = 400$ fs. The dephasing behavior and FFT amplitude differ greatly as shown in (c). The detection wavelength for all data presented is 610 nm.

Another aspect of structural dynamics on excited states is vibrational cooling. This process can be quantified by observing the rate at which mode's central frequency shifts in time. To explore this aspect, a Lorentzian line shape was fitted to the FFT spectra at different initial pump delay times T. The resulting central frequency for the C═C stretch mode is plotted against T in Figure 11a.

The C═C stretch mode shifts from 1497 to 1538 cm^{-1} at a rate of 35 fs. This rapid time constant requires further interpretation. It is too fast to be ascribed to vibrational relaxation processes on S_1, which is in the range of 400 fs according to literature.[43] Another tempting explanation can be given by assigning this remarkably fast rise to the internal conversion from S_2 to S_1. The structural rearrangement associated with a passage along such a non-adiabatic pathway in linear polyene chains is expected to occur on such a time scale.[49] However, analysis of the origin of the involved vibrations reveals a more diverse picture. As shown in Figure 11b, the amplitude decay times T_i for the C═C stretch mode differ greatly depending on the initial pump delay T. After the population has fully transferred to S_1 (transient at $T = 400$ fs in the lower panel of Figure 11b), strong vibrations with an amplitude decay time below 300 fs (see Table 1) govern the oscillatory behavior.

When considering the ultrashort lifetime (160 fs) and previous FSRS studies,[51] the vibrational dephasing time is anticipated to be even shorter for oscillations on S_2 at $T < 160$ fs. In strong contrast to such expectations, the respective amplitude decay time is above 1 ps (see transient taken at $T = 60$ fs in upper panel of Figure 11b) and cannot be fitted accurately in the detection window of 700 fs. Furthermore, the FFT spectra for initial pump delay times below $T = 120$ fs display the same properties as ground-state vibrational spectra,[17,22,32] sharp bands shifted to lower wavenumbers than the excited-state spectra and the lack of the S_1-specific C═C mode near 1800 cm^{-1} (see Figure 11c). However, these long-lived oscillations are only present when the initial pump is on, which means that the system is excited to the first optically allowed excited-state S_2. This discrepancy can only be resolved when considering an excitation mechanism alternative to the one depicted in Figure 1. In the following section on electronic population dynamics, a mechanism explaining all of the above phenomena will be elaborated. For this task, it is necessary to combine vibrational and electronic state information. Pump-DFWM turns out to be the ideal tool for this purpose because it delivers information on structural evolution and electronic population dynamics simultaneously.

2. Electronic Population Dynamics. The above discussion concentrated on pump-DFWM as a technique to monitor time-resolved excited-state vibrational dynamics. However, in contrast to absorption-based Raman techniques, the presented method also gives an opportunity to observe the changes concerning the electronic states involved. In addition to the ability to produce highly resolved vibrational spectra, this combination of examining structural and electronic population dynamics in one technique makes pump-DFWM a versatile tool for investigating the dynamics near conical intersections.[26] Considering the transient in Figure 5a, the contribution of the electronic states under investigation manifests itself in the non-oscillatory part of the signal. For analyzing the vibrational dynamics, it was necessary to subtract the slow kinetics described by $S(\tau) = A(\lambda,T)\exp[-\tau/T_d(\lambda,T)]$, with $A(\lambda,T)$ as the detection wavelength- and time-dependent pre-exponential amplitude and $T_d(\lambda,T)$ as the decay time. Accordingly, the following section will be structured as follows: after a general discussion of the slowly decaying part of the pump-DFWM signal, the pre-exponential amplitude $A(\lambda,T)$ and decay time $T_d(\lambda,T)$ will be discussed. The dependencies on detection wavelength λ and initial pump delay time T will be considered. The results will be compared to transient absorption measurements and to the conclusions drawn from the structural dynamics section with special emphasis on the role of vibrational dephasing.

2.1. General Aspects on the Slow Kinetics of the Pump-DFWM Signal: $S(\tau) = A(\lambda,T)\exp[-\tau/T_d(\lambda,T)]$. To extract the slow dynamics $S(\tau)$ from the pump-DFWM signal, a monoexponential fit to the data suffices for all values of initial pump delay T and detection wavelength λ. A plot of such monoexponential fits for different λ along the probe delay τ against T is shown in Figure 12.

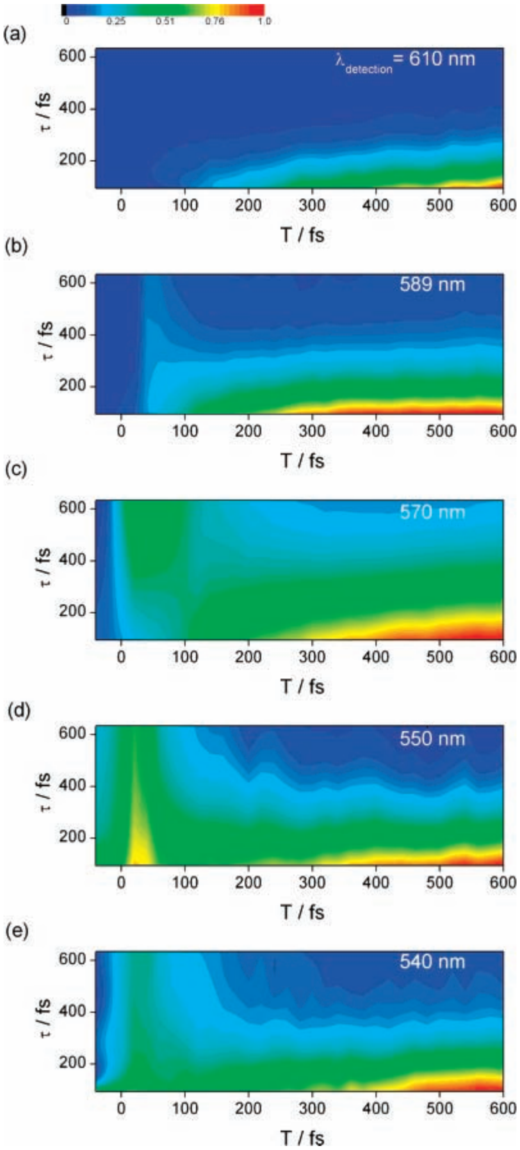

Figure 12. The slowly decaying part of the probe delay τ-transients like in Figure 5 are plotted against initial pump delay T for different detection wavelengths. The electronic population dynamics is visualized. The long-lived component for initial pump delays $T < 100$ fs is attributed to a vibrationally hot ground state. The gradual increase of the signal along T-axis is due to the relaxation of the system toward the resonantly excited S_1 state. The color code is set relative to the maximum in each plot.

Figure 12a−e shows monoexponential fits to the pump-DFWM signal at different detection wavelengths. The axis of the probe delay τ within the DFWM sequence is plotted against the initial pump delay T. This perspective allows one to observe the change in electronic structure of the investigated molecule. A common feature of all plots in Figure 12 is the slow increase of the signal along the T-axis after $T > 160$ fs. This is due to the population buildup on S_1, the state resonantly excited by the DFWM sequence. Because this condition is not fulfilled for the $S_2 \rightarrow S_m$ transition, the signal is weak for $T < 160$ fs, which means on the S_2 state, as seen in Figure 12a. In other words, the increase of the signal along the T-axis is explained by the electronic population sliding into the Franck−Condon window defined by the spectral properties of the DFWM sequence. Figure 12a already illustrates how the slowly decaying part of the pump-DFWM signal contributes to the picture of the dynamics near the conical intersection: the signal is negligible before $T < 160$ fs due to non-resonant interaction from S_2. Hence, this offset is a measure for the lifetime of this state. This value of 160 fs is in good agreement with transient absorption measurements.[52] In combination with the results presented in the previous section, this proves that pump-DFWM is a tool for the investigation of both electronic and vibrational dynamics.

In analogy to transient absorption, the variation of the detection wavelength offers a more complete view on the system's dynamics. When retaining the same excitation condi-

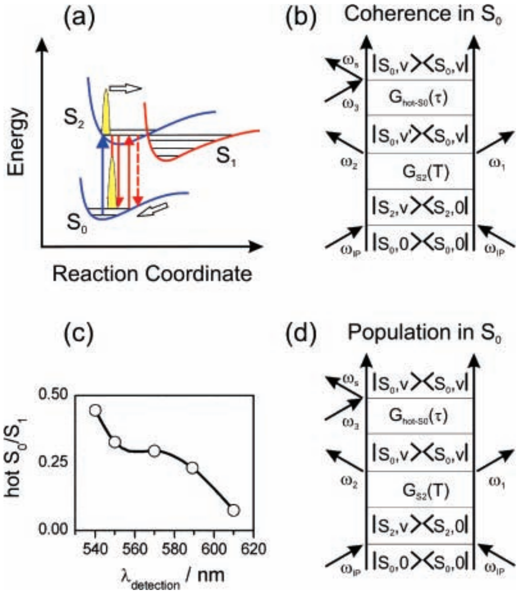

Figure 13. Excitation scheme proposed for the population of the long-lived state at short delay times T in Figures 12 and 11. Via a mechanism similar to SEP-DFWM,[12] a vibrationally hot ground state is populated with S_2 as an intermediate state. Parts (b) and (d) show the Feynman diagrams for coherence and population build in S_0, respectively. Part (c) depicts the relative contribution of the hot S_0 signal taken at $T = 80$ fs as compared to the vibrationally relaxed S_1 signal at $T = 600$ fs. The hot S_0 contribution gets stronger when the signal is detected closer to the $S_2 \rightarrow S_0$ transition around 485 nm. This provides additional support for the assignment of the long-lived feature to a hot ground state.

tion like in Figure 12a but shifting the detection wavelength to the blue (Figure 12b), the situation remains qualitatively unaltered for $T > 160$ fs. At earlier delay times, however, a signal with a long lifetime along the τ-axis occurs. This combination of short lifetime for late initial pump delays and long lifetimes for small values of T is reminiscent of the behavior of the vibrational amplitude discussed in Figure 11. Based only on vibrational dynamics data, no clear assignment of the long-lived modes at early initial pump delays could be made. In combination with the electronic dynamics, however, the mechanism depicted in Figure 13a can be proposed.

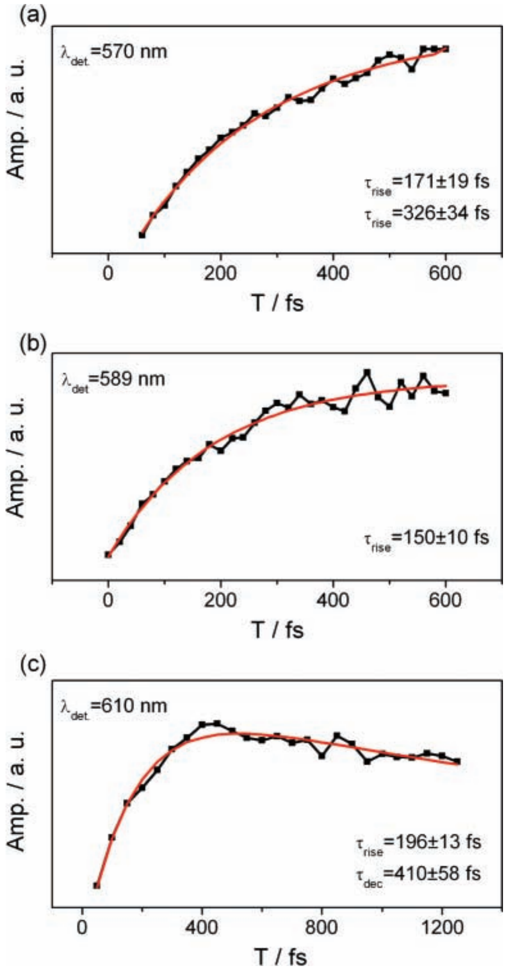

Figure 14. Fits to the pre-exponential amplitude of the pump-DFWM signal $A(\lambda,T)$ are shown for different detection wavelengths. The obtained rise and decay times correspond well with lifetimes known from transient absorption studies.

Given the long lifetime of the DFWM signal for early initial pump delay times T, a contribution of the short S_2 lifetime seems improbable. To explain this behavior, the population must be repumped to another long-lived state resonant with S_2 at the central wavelength of the DFWM sequence (560 nm). Because S_2 shows no such absorption as predicted by a semiempirical quantum chemistry calculation,[57] the population must be dumped to a vibrationally hot ground state. Such a mechanism accounts for both the long electronic and the vibrational lifetime observed. The considerable intensity of the DFWM signal is again due to resonance enhancement (see Figure 13a). The relevant Feynman diagrams are depicted in Figure 13b and d for population and coherence buildup on S_0, respectively. A similar mechanism has been exploited in the frequency domain for stimulated emission pumping DFWM (SEP DFWM),[12] aiming at the investigation of molecules in the regime of extreme rovibrational excitation. In the case of carotenoids in solution or in a protein matrix, a low lying long-lived state named S* has been previously reported and extensively discussed.[35,36,57,58] Because this Article is focused on demonstrating the capabilities of a technique, a full discussion of the nature of S* is beyond the scope of this work but will be given in a future publication. The assignment of the long-lived component at early initial pump delay times T to a hot ground state is also supported by examining the behavior of this state at different detection wavelengths. When λ is shifted further to the blue, the contribution of the hot ground state gains in intensity as compared to the S_1-related signal at $T = 600$ fs. This effect is summarized in Figure 13c. The contribution of the long-lived state is strongest when detection is shifted toward the first ground-state absorption maximum centered at 485 nm. It plays a minor role when the analyzed wavelength is further to the red. This interpretation of repumping to a vibrationally hot S_0 also explains ground-state-like properties of the FFT spectrum for initial pump delay times $T < 160$ fs as depicted in Figure 11c.

2.2. The Pre-Exponential Amplitude $A(\lambda,T)$. A phenomenological analysis of the slowly decaying part of the pump-DFWM signal $S(\tau) = A(\lambda,T) \exp[-\tau/T_d(\lambda,T)]$ showed a long-lived component for early delay times T, which was attributed to a hot ground state. This interpretation is consistent with data from the vibrational dynamics analysis. In a next step, we will analyze the pre-exponential amplitude $A(\lambda,T)$. An analogy between the discussed results and transient absorption measurements will be drawn.

Figure 14 shows show the pre-exponential amplitude $A(\lambda,T)$ against the initial pump delay T at three different detection wavelengths. The common rise constant found in all three plots corresponds well with the S_2 lifetime[28,52] and is sufficient to describe the behavior at 589 nm (Figure 14b). The longer time

TABLE 2: Decay Times $T_d(\lambda,T)$ for $T = 600$ fs at Different Detection Wavelengths

$\lambda_{\mathrm{detection}}$	610 nm	589 nm	570 nm	550 nm	540 nm
$T_d(\lambda,T)$	100 ± 3 fs	120 ± 5 fs	180 ± 10 fs	180 ± 6 fs	140 ± 7 fs

constant around 400 fs is attributed to vibrational cooling of hot S_1.[36,58,59] For detection at 610 nm, that is, in the red edge of the hot S_1 absorption,[59] this component manifests itself as a decay time. At 570 nm, a component of similar magnitude is found as one of the rise times with 66% contribution. This time constant is in good agreement with values known from pump−probe experiments.[60] Hence, the behavior of the pre-exponential amplitude in delay time T can be described consistently by the spectral properties of the early excited states in β-carotene, as is well known from transient absorption studies.[5] It has to be stressed that this is a qualitative agreement, because the time constants obtained in such experiments are exclusively determined by electronic lifetime effects. The pre-exponential factors of DFWM signals are under the additional influence of loss of vibrational coherence.[9,33] The remarkable qualitative agreement, however, between the temporal behavior of the pre-exponential amplitude and the time constants obtained in transient absorption measurements suggests that, for early delay times, the DFWM signal's amplitude is largely determined by electronic population effects rather than by pure dephasing.

2.3. The Decay Time $T_d(\lambda,T)$. The discussion of the slowly decaying part of the pump-DFWM signal $S(\tau) = A(\lambda,T)\exp[-\tau/T_d(\lambda,T)]$ will now be completed by examining the decay time $T_d(\lambda,T)$. Such decay constants were already subject to many ultrafast time-dependent four wave mixing experiments in solution.[19,33,61]

The measured decay times $T_d(\lambda,T)$ depend strongly on the detection wavelength and are summarized in Table 2. On a first impression, the wavelength dependence seems to map the electronic lifetimes of the contributing states: for red-shifted detection at 610 nm, one expects strong influence of the short-lived vibrationally hot S_1 state, resulting in a short $T_d(\lambda,T)$. Accordingly, the decay times increase when detection takes place closer to the bottom of the S_1 potential well. Such a relationship between the electronic lifetime and the decay time of the DFWM signal was already reported for *trans*-stilbene,[19] where even on variation of the solvent, the DFWM decay time matched the population lifetime as measured in a transient absorption experiment. In the case of β-carotene, however, this quantitative correlation breaks down: The measured DFWM decay times as shown in Table 2 are all below 200 fs. The electronic lifetimes of the contributing states, such as 400 fs for vibrationally hot S_1 and 9 ps for S_1 after relaxation, are all considerably above these values.

As discussed in the theoretical basis section and expressed in detail in a work by Joo and Albrecht,[33] the terms contributing to $T_d(\lambda,T)$ can be identified as the decay time related to the upper state electronic lifetime $T_{1,\mathrm{S}n}/2$, the decay time of the population in the excited vibronic level $T_{1,\mathrm{S}n,\upsilon}/2$, and the dephasing times for vibrational coherences on upper and lower electronic state $T_{2,\mathrm{S}n,\upsilon}/2$ and $T_{2,\mathrm{S}1,\upsilon}/2$. The latter can be obtained from the time-domain evolutionary fitting analysis presented in Table 1. The aim of the following paragraph is to estimate the importance of the contributing terms mentioned above for the overall decay time $T_d(\lambda,T)$.

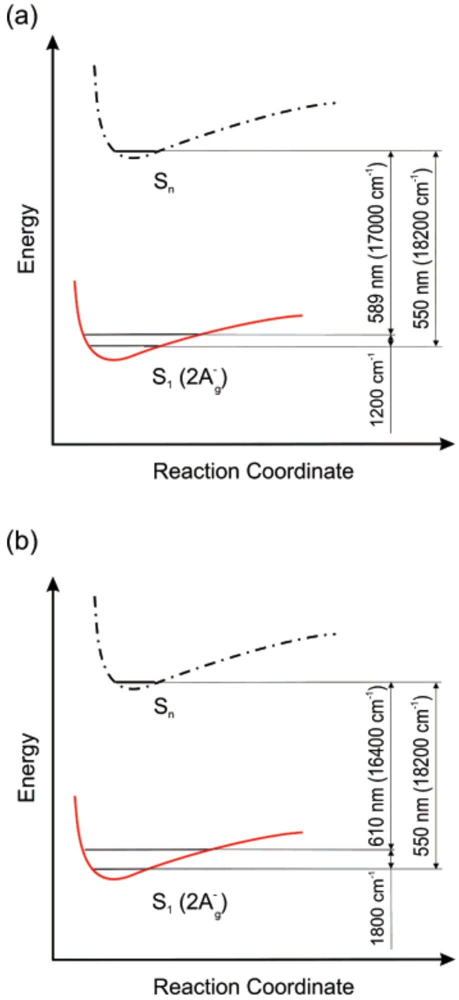

Figure 15. Sketches of the potential energy curves of β-carotene, illustrating the relation between detection wavelength and the vibrational mode dominating the dephasing behavior. The energy spacings for detection at 589 nm (a) and 610 nm (b) detection wavelength are shown. The respective difference from the minimum of the S_1 potential energy well at 550 nm (18 200 cm^{-1}) indicates which mode contributes to the overall decay time $T_d(\lambda,T)$.

The shortest time constant in Table 2 is 100 fs for detection at 610 nm. This fast decay suggests that the DFWM transients are governed by the most rapid process listed above, which is vibrational dephasing on S_1. Contributions from S_n can be neglected for the chosen initial pump delay time $T = 600$ fs, because the electronic lifetime of the respective state is significantly shorter: a fit to the recovery dynamics in Figure 4b revealed a time constant of 310 fs for the internal conversion between S_n and S_1. For earlier initial delay times T, contributions from both S_n and hot S_1 dephasing rates may contribute to the overall decay time $T_d(\lambda,T)$. When considering the effects of vibrational dephasing on the electronic dynamics discussed here, the question arises whether any connection between the values for $T_d(\lambda,T)$ in Table 2 and the amplitude decay times summarized in Table 1 in the vibrational dynamics section can be made. This is plausible because those parameters describe the same physical process, vibrational dephasing. All modes in Table 1 exhibit specific amplitude decay constants, which raises the following problem: which mode dominates the vibrational dephasing behavior at a specific detection wavelength, influencing the DFWM signal's non-oscillatory decay? This can be resolved by regarding the energy spacing between the detection wavelength in question and the bottom of the S_1 potential energy surface at 550 nm as sketched in Figure 15: for example, 589 nm (16 978 cm^{-1}) is 1203 cm^{-1} detuned from the lowest lying absorption on S_1 (550 nm or 18 182 cm^{-1}), which corresponds well to the value for the C−C stretch mode (1150 cm^{-1}), as can be seen in Figure 15a. Hence, the $\upsilon = 1$ state of this mode is preferably detected at 589 nm and determines the slow kinetics decay time $T_\mathrm{d}(\lambda,T)$. Indeed, the measured T_d(589 nm, 600 fs) = 120 ± 5 fs is in good agreement with the expectation based on the vibrational dephasing time from Table 1, $T_{2,\mathrm{S}1,\nu}/2 = 135$ fs. Following the same argument, T_d(610 nm, 600 fs) = 100 fs cannot be attributed to dephasing of the mode dominating the behavior at 589 nm detection wavelength. The energy difference between 610 nm (16 393 cm^{-1}) and the potential's minimum is 1788 cm^{-1} (see Figure 15b), which coincides with the value for the S_1-specific mode near 1800 cm^{-1}. According to Table 1, one-half of the amplitude decay time is $T_{2,\mathrm{S}1,\nu}/2 = 77$ fs, which is in reasonable agreement with the observed value for $T_\mathrm{d}(\lambda,T) = 100$ fs.

The values for $T_\mathrm{d}(\lambda,T)$ shift to larger values when going closer to the S_1-absorption maximum near 560 nm and decrease again for blue-shifted detection at 540 nm. The values around 180 fs seem too high to be dominated only by vibrational dephasing. Slower processes like lifetime-induced decay of S_1 ($T_{1,\mathrm{S}1} = 9$ ps) may start to give minor contributions at blue-shifted detection.

In summary, the time scale of the slowly decaying component of $T_\mathrm{d}(\lambda,T)$ for β-carotene in cyclohexane cannot be explained only by electronic population dynamics, like it was possible for other solvated molecules with longer S_n lifetimes.[19] Only by employing a versatile tool like pump-DFWM, which allows for simultaneous wavelength dispersed detection of vibrational and electronic dynamics, one can dissect the monoexponential decay into contributions from diagonal (population rates) and off-diagonal (vibronic dephasing rates) elements of the respective density matrix. Upon examination of the energy spacings at certain detection wavelengths, the conclusion can be drawn that vibrational dephasing determines the slow decaying behavior of the DFWM signal.

Conclusions

The combination of high spectral (10 cm^{-1}) and temporal resolution (20 fs) makes pump-DFWM an ideal tool for studying vibrational dynamics on molecular excited states, matching the benchmarks set by time-resolved stimulated Raman techniques.[23,25] In addition to the latter methods, the results obtained from pump-DFWM are more comprehensive due to the possibility to spectrally disperse the signal and hence to simultaneously obtain information from different Franck−Condon regions of the excited-state surface. Especially when exploring the dynamics near decisive points like conical intersections, pump-DFWM is expected to give rise to valuable new experimental insights because this technique allows for observing the interplay between structural and electronic dynamics. Furthermore, the pure time domain character of the method makes it a perfectly suited candidate for the coherent control of excited-state processes.

Acknowledgment. We thank Bernhard von Vacano for valuable discussions and M. Hill for assistance in the lab. Support by the Max-Planck Society is gratefully acknowledged.

References and Notes

(1) Bowman, R. M.; Dantus, M.; Zewail, A. H. *Chem. Phys. Lett.* **1989**, *156*, 131.

(2) Baumert, T.; Grosser, M.; Thalweiser, R.; Gerber, G. *Phys. Rev. Lett.* **1991**, *67*, 3753.

(3) Fragnito, H. L.; Bigot, J. Y.; Becker, P. C.; Shank, C. V. *Chem. Phys. Lett.* **1989**, *160*, 101.

(4) Wurzer, A. J.; Lochbrunner, S.; Riedle, E. *Appl. Phys. B* **2000**, *71*, 405.

(5) Cerullo, G.; Lanzani, G.; Zavelani-Rossi, M.; De Silvestri, S. *Phys. Rev. B* **2001**, *6324*, 4.

(6) Kaiser, W. e. *Top. Appl. Phys.* **1992**, 60.

(7) Bardeen, C.; Wang, Q.; Shank, C. V. *Abstr. Pap. Am. Chem. Soc.* **1995**, *209*, 128.

(8) Malkmus, S.; Durr, R.; Sobotta, C.; Pulvermacher, H.; Zinth, W.; Braun, M. *J. Phys. Chem. A* **2005**, *109*, 10488.

(9) Butcher, P. N.; Cotter, D. *The Elements of Nonlinear Optics*; University of Cambridge: MA, 1990.

(10) Motzkus, M.; Pedersen, S.; Zewail, A. H. *J. Phys. Chem.* **1996**, *100*, 5620.

(11) Pastirk, I.; Brown, E. J.; Grimberg, B. I.; Lozovoy, V. V.; Dantus, M. *Faraday Discuss.* **1999**, 401.

(12) Vaccaro, P. H. *Advanced Series in Physical Chemistry: Molecular Dynamics and Spectroscopy by Stimulated Emission Pumping*; World Scientific Publishers: New York, 1994.

(13) Mukamel, S. *Nonlinear Optical Spectroscopy*; University Press: Oxford, 1995.

(14) Underwood, D. F.; Blank, D. A. *J. Phys. Chem. A* **2003**, *107*, 9736.

(15) Schmitt, M.; Knopp, G.; Materny, A.; Kiefer, W. *Chem. Phys. Lett.* **1997**, *270*, 9.

(16) Brown, E. J.; Zhang, Q. G.; Dantus, M. *J. Chem. Phys.* **1999**, *110*, 5772.

(17) Siebert, T.; Maksimenka, R.; Materny, A.; Engel, V.; Kiefer, W.; Schmitt, M. *J. Raman Spectrosc.* **2002**, *33*, 844.

(18) Hornung, T.; Skenderovic, H.; Motzkus, M. *Chem. Phys. Lett.* **2005**, *402*, 283.

(19) Fujiyoshi, S.; Takeuchi, S.; Tahara, T. *J. Phys. Chem. A* **2003**, *107*, 494.

(20) Oberle, J.; Jonusauskas, G.; Abraham, E.; Rulliere, C. *Chem. Phys. Lett.* **1995**, *241*, 281.

(21) Oberle, J.; Jonusauskas, G.; Abraham, E.; Rulliere, C. *Opt. Commun.* **1996**, *124*, 616.

(22) Siebert, T.; Schmitt, M.; Engel, V.; Materny, A.; Kiefer, W. *J. Am. Chem. Soc.* **2002**, *124*, 6242.

(23) Yoshizawa, M.; Kurosawa, M. *Phys. Rev. A* **2000**, *61*, 013808.

(24) Fujiyoshi, S.; Ishibashi, T.; Onishi, H. *J. Phys. Chem. A* **2004**, *108*, 11165.

(25) Kukura, P.; McCamant, D. W.; Mathies, R. A. *Annu. Rev. Phys. Chem.* **2006**, *58*, 461.

(26) Garavelli, M.; Bernardi, F.; Olivucci, M.; Vreven, T.; Klein, S.; Celani, P.; Robb, M. A. *Faraday Discuss.* **1998**, 51.

(27) Domcke, W.; Stock, G. *Advances in Physical Chemistry*; Wiley: New York, 1997.

(28) Polivka, T.; Sundstrom, V. *Chem. Rev.* **2004**, *104*, 2021.

(29) Dobryakov, A. L.; Kovalenko, S. A.; Ernsting, N. P. *J. Chem. Phys.* **2005**, *123*, 044502.

(30) Beadie, G.; Bashkansky, M.; Reintjes, J.; Scully, M. O. *J. Mod. Opt.* **2004**, *51*, 2627.

(31) Mehendale, M.; Giordmaine, J. A.; Gatzogiannis, E.; Dogariu, A.; Warren, W. S.; Beadie, G.; Scully, M. O. *Opt. Lett.* **2006**, *31*, 256.

(32) Hauer, J.; Skenderovic, H.; Kompa, K. L.; Motzkus, M. *Chem. Phys. Lett.* **2006**, *421*, 523.

(33) Joo, T.; Albrecht, A. C. *Chem. Phys.* **1993**, *173*, 17.

(34) Larsen, D. S.; Papagiannakis, E.; van Stokkum, I. H. M.; Vengris, M.; Kennis, J. T. M.; van Grondelle, R. *Chem. Phys. Lett.* **2003**, *381*, 733.

(35) Wohlleben, W.; Buckup, T.; Hashimoto, H.; Cogdell, R. J.; Herek, J. L.; Motzkus, M. *J. Phys. Chem. B* **2004**, *108*, 3320.

(36) Buckup, T.; Savolainen, J.; Wohlleben, W.; Herek, J. L.; Hashimoto, H.; Correia, R. R. B.; Motzkus, M. *J. Chem. Phys.* **2006**, *125*, 199505.

(37) Dudovich, N.; Dayan, B.; Faeder, S. M. G.; Silberberg, Y. *Phys. Rev. Lett.* **2001**, *86*, 47.

(38) Lang, T.; Motzkus, M.; Frey, H. M.; Beaud, P. *J. Chem. Phys.* **2001**, *115*, 5418.

(39) Prince, B. D.; Chakraborty, A.; Prince, B. M.; Stauffer, H. U. *J. Chem. Phys.* **2006**, *125*, 044502.

(40) Siebert, T.; Schmitt, M.; Michelis, T.; Materny, A.; Kiefer, W. *J. Raman Spectrosc.* **1999**, *30*, 807.

(41) Nelson, K. A.; Casalegno, R.; Miller, R. J. D.; Fayer, M. D. *J. Chem. Phys.* **1982**, *77*, 1144.

(42) Schlucker, S.; Szeghalmi, A.; Schmitt, M.; Popp, J.; Kiefer, W. *J. Raman Spectrosc.* **2003**, *34*, 413.

(43) McCamant, D. W.; Kukura, P.; Mathies, R. A. *J. Phys. Chem. A* **2003**, *107*, 8208.

(44) Shimada, R.; Kano, H.; Hamaguchi, H. *J. Raman Spectrosc.* **2006**, *37*, 469.

(45) Herek, J. L.; Wohlleben, W.; Cogdell, R. J.; Zeidler, D.; Motzkus, M. *Nature* **2002**, *417*, 533.

(46) Prokhorenko, V. I.; Nagy, A. M.; Waschuk, S. A.; Brown, L. S.; Birge, R. R.; Miller, R. J. D. *Science* **2006**, *313*, 1257.

(47) Wohlleben, W.; Buckup, T.; Herek, J. L.; Cogdell, R. J.; Motzkus, M. *Biophys. J.* **2003**, *85*, 442.

(48) McCamant, D. W.; Kim, J. E.; Mathies, R. A. *J. Phys. Chem. A* **2002**, *106*, 6030.

(49) Garavelli, M.; Smith, B. R.; Bearpark, M. J.; Bernardi, F.; Olivucci, M.; Robb, M. A. *J. Am. Chem. Soc.* **2000**, *122*, 5568.

(50) Fuss, W.; Haas, Y.; Zilberg, S. *Chem. Phys.* **2000**, *259*, 273.

(51) Kukura, P.; McCamant, D. W.; Mathies, R. A. *J. Phys. Chem. A* **2004**, *108*, 5921.

(52) Zhang, J. P.; Skibsted, L. H.; Fujii, R.; Koyama, Y. *Photochem. Photobiol.* **2001**, *73*, 219.

(53) Kosumi, D.; Komukai, M.; Hashimoto, H.; Yoshizawa, M. *Phys. Rev. Lett.* **2005**, *95*, 213601.

(54) Garavelli, M.; Celani, P.; Bernardi, F.; Robb, M. A.; Olivucci, M. *J. Am. Chem. Soc.* **1997**, *119*, 11487.

(55) Cerullo, G.; Polli, D.; Lanzani, G.; De Silvestri, S.; Hashimoto, H.; Cogdell, R. J. *Science* **2002**, *298*, 2395.

(56) Rondonuwu, F. S.; Kakitani, Y.; Tamura, H.; Koyama, Y. *Chem. Phys. Lett.* **2006**, *429*, 234.

(57) Niedzwiedzki, D. M.; Sullivan, J. O.; Polivka, T.; Birge, R. R.; Frank, H. A. *J. Phys. Chem. B* **2006**, *110*, 22872.

(58) Andersson, P. O.; Gillbro, T. *J. Chem. Phys.* **1995**, *103*, 2509.

(59) de Weerd, F. L.; van Stokkum, I. H. M.; van Grondelle, R. *Chem. Phys. Lett.* **2002**, *354*, 38.

(60) Yoshizawa, M.; Aoki, H.; Hashimoto, H. *Phys. Rev. B* **2001**, *63*, 180301.

(61) Vierheilig, A.; Chen, T.; Waltner, P.; Kiefer, W.; Materny, A.; Zewail, A. H. *Chem. Phys. Lett.* **1999**, *312*, 349.